LAWRENCE
LIVERMORE
NATIONAL
LABORATORY

LLNL-CONF-686162

CT Dual-energy Decomposition into X-ray Signatures Rho-e and Z-e

H. E. Martz, I. M. Seetho, K. M. Champley, J. A. Smith, S. G. Azevedo

March 16, 2016

SPIE Anomaly Detection and Imaging with X-Rays (ADIX)
Baltimore, MD, United States
April 17, 2016 through April 21, 2016

Disclaimer

CT Dual-energy Decomposition into X-ray Signatures ρ_e and Z_e

(Invited Paper[*]*)*

Harry E. Martz, Jr., Isaac M. Seetho, Kyle M. Champley, Jerel A. Smith, Stephen G. Azevedo
Lawrence Livermore National Laboratory, P. O. Box 808, L-154, Livermore, CA, USA 94551

ABSTRACT

In a recent journal article [IEEE Trans. Nuc. Sci., 63(1), 341-350, 2016], we introduced a novel method that decomposes dual-energy X-ray CT (DECT) data into electron density (ρ_e) and a new effective-atomic-number called Z_e in pursuit of system-independent characterization of materials. The Z_e of a material, unlike the traditional Z_{eff}, is defined relative to the actual X-ray absorption properties of the constituent atoms in the material, which are based on published X-ray cross sections. Our DECT method, called SIRZ (System-Independent ρ_e/Z_e), uses a set of well-known reference materials and an understanding of the system spectral response to produce accurate and precise estimates of the X-ray-relevant basis variables (ρ_e, Z_e) regardless of scanner or spectra in diagnostic energy ranges (30 to 200 keV). Potentially, SIRZ can account for and correct spectral changes in a scanner over time and, because the system spectral response is included in the technique, additional beam-hardening correction is not needed. Results show accuracy (<3%) and precision (<2%) values that are much better than prior methods on a wide range of spectra. In this paper, we will describe how to convert DECT system output into (ρ_e, Z_e) features and we present our latest SIRZ results compared with ground truth for a set of materials.

Keywords: Dual-energy computed tomography, effective atomic number, electron density, x-ray characterization, photoelectric-compton decomposition, system-independent CT

1. INTRODUCTION

Identifying internal objects or anomalies inside material specimens that are about a meter in diameter, such as humans[1] or checked baggage[2] or many nondestructive characterization (NDC) examples[3-4], can be performed in a quantitative way with dual-energy X-ray computed tomography (DECT)[5-8]. The two spectral energy ranges employed in the DECT tomographic scans provide a rough two-parameter basis set or feature space that can characterize physical values of each 3D volume element (voxel) in the specimen. Traditional methods attempt to use feature spaces related to the material density, ρ (that trends with the high-energy attenuation coefficient), and effective atomic number (approximated by Z_{eff}[9] or the ratio of low- to high-energy attenuation coefficient)[8]. These empirically-estimated features are derived from manipulations of high- and low-energy linear attenuation coefficients (LACs), which can be problematic because LAC values are dependent on the energy spectra used for the scans such that results from scanning the same object can vary between different scanners using different spectral responses and over time as a scanner ages. A more descriptively-useful feature space is one that removes the spectral dependence of the results. We propose such a space, which uses the basis variables of electron density (ρ_e) and a new effective atomic number Z_e derived from material X-ray cross sections.

We have developed a new method for system-independent DECT processing using the (ρ_e, Z_e) feature space called SIRZ (System-Independent ρ_e/Z_e) that has been demonstrated to provide accurate and precise characterization over a range of scanners and spectra[8]. More recent experiments have confirmed the earlier results and led to development of a rigorous SIRZ implementation at the Lawrence Livermore National Laboratory (LLNL), which is now undergoing verification and validation for the DECT scanners built and deployed at LLNL. The SIRZ algorithm and supporting processing tools have been aggregated into a software suite called Livermore Tomography Tools (LTT)[10]. Our aim is to encourage wide-

[*] Manuscript submitted to SPIE Anomaly Detection and Imaging with X-Rays (ADIX) Paper 9847-12, Tracking No. SI16D-DS133-34, on March 18, 2016. LLNL Release number LLNL-CONF-686162. This work was funded by the Science and Technology Directorate of the Department of Homeland Security (DHS). This work performed under the auspices of the U.S. Department of Energy by Lawrence Livermore National Laboratory under Contract DE-AC52-07NA27344.

spread use of SIRZ for anomaly detection and identification in many DECT applications, and to continue verification of this method across other scanners, spectra and specimens.

In this paper, we describe the SIRZ method in general, its implementation in LTT for automated processing, and recent results on DECT data. Our goals include applying the SIRZ method to diverse scanners and applications across the NDC and security domains. We identify directions for future research and development into quantitative system-independent material characterization using DECT.

2. SYSTEM-INDEPENDENT DECT WITH SIRZ

In this section, we give a brief introduction to SIRZ, describe the scanning requirements for obtaining accurate and precise ρ_e and Z_e results (using the system spectral response and a set of reference materials), show how SIRZ has been automated by its implementation in LTT, and summarize the preprocessing steps needed. The ρ_e and Z_e features are used because they both are independent of the DECT scanner and spectral response, and they are directly related to X-ray attenuation properties of materials—absorption is directly proportional to ρ_e, and the definition of Z_e includes the total X-ray cross section from known tables[11].

2.1 SIRZ Algorithm

The SIRZ algorithm is shown in the flow diagram in Figure 1, and a more formal mathematical definition is found in the original paper[8]. From the high- and low-energy sinograms produced by the scanner (P_H and P_L at left), the common processing methods involve CT reconstruction (by filtered backprojection, FBP, or equivalent) into high- and low-energy images of LAC's (μ_{high} and μ_{low}). It is then straightforward to transform these data into feature spaces of either (μ_{high}, μ_{low}/μ_{high}) for the Ratio method[5] or (μ_{high}, Z_{eff}) by calculating Z_{eff} through simple interpolation[12] or with more complex methods[2]. These methods yield results that approximate a material's physical properties of density (with μ_{high}) and atomic number (with μ_{low}/μ_{high} or Z_{eff}).

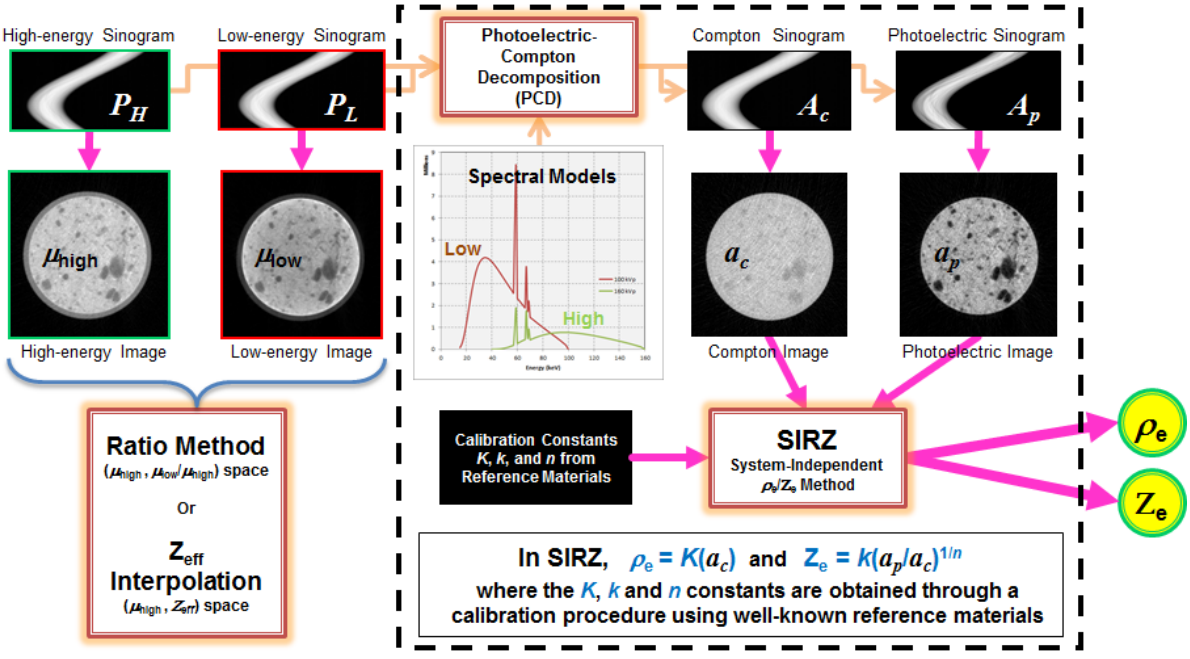

Figure 1. A flow diagram of the SIRZ algorithm compared to the Ratio and Z_{eff}-interpolation methods of processing DECT data. See text for details.

The SIRZ method (in the dashed box) processes the same low- and high-energy sinograms through a three-step process of photoelectric-Compton decomposition (PCD), reconstruction into Compton and photoelectric attenuation component images, and conversion to the (ρ_e, Z_e) feature space. Validity of the PCD was established by Alvarez and Macovski[5] (A&M), who showed that spectrally-dependent dual-energy attenuation coefficients can be approximately decomposed into Compton scatter (A_c) and photoelectric absorption (A_p) components that provide energy-independent representations of physical X-ray absorption over a broad energy range (30 to 200 keV) where photoelectric and Compton effects dominate. The PCD process requires knowledge of the *system spectral response* defined as the product of the X-ray source spectrum and source filters, and the detector spectral response for low- and high-energy spectra. Then the A_c and A_p sinograms can be reconstructed by FBP to form Compton (a_c) and photoelectric (a_p) images of electron density. The final SIRZ step involves conversion to the (ρ_e, Z_e) features, which follows from estimates of X-ray absorption, also introduced by A&M as follows:

$$\rho_e = K a_c \tag{1}$$

and

$$Z_e = k\left(\frac{a_p}{a_c}\right)^{1/n}, \tag{2}$$

where K, k and n are constant coefficients that are found by calibration against a set of reference materials (at least three) with known ρ_e and Z_e values. A software package called ZeCalc[13], which was developed by LLNL and is available under limited license by DHS, calculates optimal estimates of ρ_e and Z_e for a material of known chemical composition with known density and a specified energy range (from 10 to 500 keV for ZeCalc). There can be spectral fit inaccuracies near material absorption edges, so ZeCalc also displays the system spectral response compared to the transmission spectrum to make the user aware of possible estimation errors.

Selections of system spectral response models, and of the reference materials employed, are important aspects of SIRZ that are discussed in the next two subsections.

2.2 System Spectral Response

To have an accurate representation of the materials, SIRZ needs a good estimate of the system spectral response. Source and detector spectral models are best estimated with knowledge of the hardware involved, e.g., source anode material, take-off angle, X-ray filtration materials and thicknesses, and detector specifications. Obtaining such information from the manufacturers is useful; however, spectral responses can also be estimated from the X-ray signatures of known reference materials (see the next section). We found that spectral models from the software program SpekCalc[14] were sufficiently accurate as starting estimates for a given endpoint voltage, as were others[15-16]. For the experimental work described in Section 3, the spectral response models for each energy range were initially estimated with SpekCalc using manufacturers' specifications. Each estimated spectrum was then optimized by making small adjustments in the modeled source filtration such that the transmission for the overall system spectral response, including the detector, matched the experimentally-measured transmissions for a set of known specimens with a broad range of Z_e, ρ_e, and attenuation values. This added filtration was primarily needed to adjust for unknown quantities in the system (for example, a manufactured plate of unknown composition on the front of the detector panel).

2.3 Reference Materials

The choice of reference materials is important for any SIRZ application since these references establish the range in feature space for which specimen characteristics can be interpolated (rather than extrapolated). This choice is therefore influenced by the ranges of ρ_e and Z_e values in the specimens to be scanned. In our case, we chose the reference materials to span the (ρ_e, Z_e) feature space of interest to security and NDC applications. They were high-purity (typically of a single element or of well-known elemental and molecular composition) such that actual ρ_e and Z_e values could be reliably calculated using ZeCalc. Table 1 lists the reference materials and their chemical and physical properties. The ρ_e values were from 0.55 to 1.16 moles-e^-/cm^3, and the Z_e values were from 6 to 14. Like the test specimens used in our experiments, the reference materials were independently certified with purity and trace element analyses.

Table 1. Reference materials scanned in the DECT experiments.

Reference Material	Chemical Makeup	Bulk Density, ρ (g/cc)	Electron Density[b], ρ_e (moles-e^-/cm^3)	Effective Atomic Number[b], Z_e
Graphite	C	1.80 ± 0.01	0.901 ± 0.003	6.00 ± 0.01
POM	$(CH_2O)_n$	1.40 ± 0.01	0.748 ± 0.003	7.01 ± 0.01
Water [a]	H_2O	1.00 ± 0.01	0.554 ± 0.002	7.43 ± 0.01
PTFE	$(C_2F_4)_n$	2.18 ± 0.02	1.044 ± 0.003	8.44 ± 0.01
Magnesium	Mg	1.74 ± 0.02	0.857 ± 0.003	12.00 ± 0.01
Silicon	Si	2.33 ± 0.02	1.162 ± 0.003	14.00 ± 0.01

[a] De-ionized reagent-grade water (from Fisher Scientific, Cat # 23-751-610) is contained in a polyethylene bottle.
[b] Z_e and ρ_e values are supplied by ZeCalc[13] using a 160 keV endpoint spectrum and a nominal areal density of 2.5 g/cm^2.

Note that our current work uses six reference materials as opposed to the four used in our previous studies[8]. While the results are the same within error bounds across our studies, six materials provide redundancy to the experiments. We use the abbreviation POM for polyoxymethylene, an acetyl copolymer resin that is similar to the acetyl homopolymer known by the brand name Delrin by DuPont Co. Likewise, we use PTFE as an abbreviation for polytetrafluoroethylene, which is a synthetic fluoropolymer of tetrafluoroethylene that is identical in composition to Teflon by DuPont Co. It is important to note that the X-ray attenuation properties of PTFE can change the more it is irradiated[17]. We are exploring other materials to use as references that have more radiation tolerance, such as fluorinated ethylene propylene.

The DECT scanners used in SIRZ testing produced data for the reference materials simultaneously with the specimen, but this need not be the case if the spectral response is stable. Instead, the reference materials could be measured periodically as a calibration procedure. How often the system needs to be calibrated in this way to account for spectral changes over time is a scanner-specific issue. However, the SIRZ-estimated values of the *K*, *k* and *n* coefficients, and therefore the ρ_e and Z_e values for the reference materials, remained constant (within measurement error) for the entire six-week experimental cycle on the LLNL scanner.

2.4 SIRZ Implementation in LTT

LLNL has access to a wide range of X-ray scanners, each with different X-ray sources, detectors, geometries, fields of view, etc., to address imaging applications in various domains. To analyze results from these scanners, we have developed the Livermore Tomography Tools software suite[10] to allow efficient and accurate processing of radiographic data from any scanner using a variety of computational platforms. LTT contains a collection of CT algorithms written in C/C++ so that it can be used across platforms (Windows, Mac, Linux). It is implemented to utilize multi-threaded architectures (OpenMP) and GPU processing (OpenCL) where available. Many algorithms, including novel and state-of-the-art ones[18-20], are included so that LTT is capable of processing CT data from raw detector counts to reconstructed images while supporting most conventional scanner geometries (parallel, fan, or cone beam) and modern fixed-gantry systems. Data sets that are too large to fit into memory are processed in smaller portions and can be split across parallel processors. Simulation capabilities of X-ray cross sections, spectral distributions and CT data of various types also exist in LTT. For data visualization, LTT has cross-communication with the ImageJ software[21] from the U. S. National Institutes of Health.

SIRZ has recently been implemented into the LTT environment and is now under-going extensive verification with respect to many years of collected DECT data in the LLNL archives. Where possible, a goal of LTT is to provide quantitatively-accurate results (with specified units) in a timely manner. For DECT, SIRZ is designed with this goal in mind. The NDC scanners that are in active use at LLNL are being updated to acquire data compatible with the SIRZ algorithm in LTT for automated processing. To date, the results from the LTT implementation of an automated SIRZ matches prior R&D results and are consistent with the expected performance for accurate and precise material characterization. Results shown in this paper are from the automated LTT implementation of SIRZ.

2.5 Preprocessing Steps for SIRZ

Depending on the peculiarities of each DECT scanner, there can be a number of data preprocessing steps needed to generate the high- and low-energy sinograms (P_H and P_L) at the start of Figure 1. Typically these steps are applied to remove artifacts that are inherent in the data acquisition process and, for best results, are performed in the reverse order

in which those artifacts become physically introduced into the raw signals. For the particular scanner type used in this study (collimated source, rotated specimen, 2D flat-panel X-ray detector), we have found that the following order of pre-processing steps roughly produces the best artifact corrections: (1) bad-pixel correction, (2) gain correction on a per-pixel basis, (3) deblurring of the 2D pixel-to-pixel blur in the detector, (4) scatter correction based on a model of X-ray propagation, (5) conversion to log-attenuation values, and (6) level balancing across projection angles to address ghosting issues caused by detector persistence. These steps in this order are employed in the LLNL systems that perform the SIRZ decomposition, reconstruction and conversion to (ρ_e, Z_e) features. Without describing each step explicitly, the data reported in this paper follow the above pre-processing steps in the order listed.

Notice that beam-hardening compensation, which is normally needed for broad-spectrum X-ray applications, is not needed with SIRZ because the spectral information is inherent in the algorithm[8]. This fact that the system spectral response is incorporated into the SIRZ algorithm serves to reduce the beam-hardening error and to streamline the analysis.

3. SIRZ TEST RESULTS

In our original R&D work[8], we demonstrated the consistency of SIRZ through a series of R&D experiments on two different scanners with widely-varying spectra. Since that first demonstration of SIRZ, more extensive testing has been done to assess SIRZ performance under varying conditions. This section describes some of the recent tests and their outcomes.

3.1 DECT Scanner Used in Testing

A recently-upgraded DECT scanner built for NDC and security studies at LLNL was selected to assess our ability to apply an automated SIRZ in LTT to a new system. This scanner was a different physical implementation of the same basic design that was introduced in previous R&D experiments[8]. It had a fixed source-detector geometry with identical dual-level rotating "carousels" (for specimen on top and reference materials below) and the same type of X-ray tube source (Yxlon 450 kV D09 tube-head with tungsten target, 11-degree takeoff angle, 0.4-mm spot size, and 5.0-mm beryllium window). The main difference between prior systems was in a new detector used, which was a PerkinElmer XRD 1620 flat-panel amorphous-silicon detector with 2048×2048 detector elements of size 0.200 mm × 0.200 mm, and a DRZ Plus Gd_2O_2S:Tb scintillator. At each projection angle, the full 2D set of detector elements were reduced to two linear (1D) projections through (1) the specimen and (2) the set of reference materials, which were scanned simultaneously as the dual-level carousel rotated.

Our experiments focused on scans with two commonly-used spectral pairs of 100-keV and 160-keV endpoint energies. The X-ray source filters were 1.94-mm of aluminum for 100-keV scans and 1.94-mm of aluminum and 1.85-mm of copper for 160-kV scans. Two complete 360-degree rotations consisting of 720 stepped projections were performed for each of the two source-energy filtered spectra.

3.2 Recent SIRZ Results

A set of well-characterized specimens of different diameters (listed in Table 2) were scanned on the above DECT scanner and reconstructed through the automated LTT version of SIRZ. Some of the specimens (e.g., aluminum) are different from the reference materials and from the R&D set; however, they all were carefully constructed and measured so that the true values of (ρ_e, Z_e) were known and referred to as ground truth (the "Actual" columns). The accuracy results are tabulated in Table 2 as the absolute error of the estimates of ρ_e and Z_e from their known values, as well as the average error in percent for each estimate.

The (ρ_e, Z_e) feature space with each of these specimens plotted on the same graph is shown in Figure 2. The LTT-automated SIRZ results had an average (ρ_e, Z_e) accuracy error of <1% for all specimens. (Precision scores were not available due to the small sample size.) The higher-attenuating specimens (magnesium, large PTFE, and aluminum) demonstrated the highest ρ_e error, while all were still consistent with the <3% level from prior studies. All individual accuracy errors for Z_e were below 2%. From these results, we conclude that the automated version of SIRZ in LTT performs similarly to prior tests and reinforces our claims that SIRZ provides system-independent measurements of physical properties.

Table 2. SIRZ accuracy (error from "actual" values as calculated by ZeCalc in %) for the specimens.

Specimen Material (Diameter)	ρ_e			Z_e		
	Actual [b]	Mean [c]	Error % [d]	Actual [b]	Mean [c]	Error % [d]
PTFE (2")	1.044	1.058	1.30%	8.44	8.365	-0.89%
PTFE (1")	1.044	1.037	-0.67%	8.44	8.384	-0.66%
Silicon (1")	1.162	1.168	0.48%	14	13.797	-1.45%
Silicon (1")	1.162	1.170	0.68%	14	13.798	-1.44%
Magnesium (1")	0.857	0.871	1.59%	12	12.081	0.68%
Water [a] (1")	0.554	0.552	-0.44%	7.43	7.422	-0.11%
Graphite (1")	0.862	0.861	-0.14%	6	6.041	0.69%
Aluminum (1")	1.302	1.332	2.28%	13	13.093	0.71%
POM (2")	0.748	0.747	-0.13%	7.01	6.888	-1.74%
Average error			0.55%			-0.47%

[a] De-ionized reagent-grade water (from Fisher Scientific, Cat # 23-751-610) was contained in a polyethylene bottle.
[b] The ρ_e, and Z_e "Actual" values supplied by ZeCalc[13] using a 160-keV endpoint spectrum and a nominal areal density of 2.5 g/cm^2.
[c] The ρ_e, and Z_e "Mean" estimated values supplied by the automated SIRZ algorithm in LTT[10].
[d] "Error %" values calculated as [(Mean-Actual)/Actual] × 100.

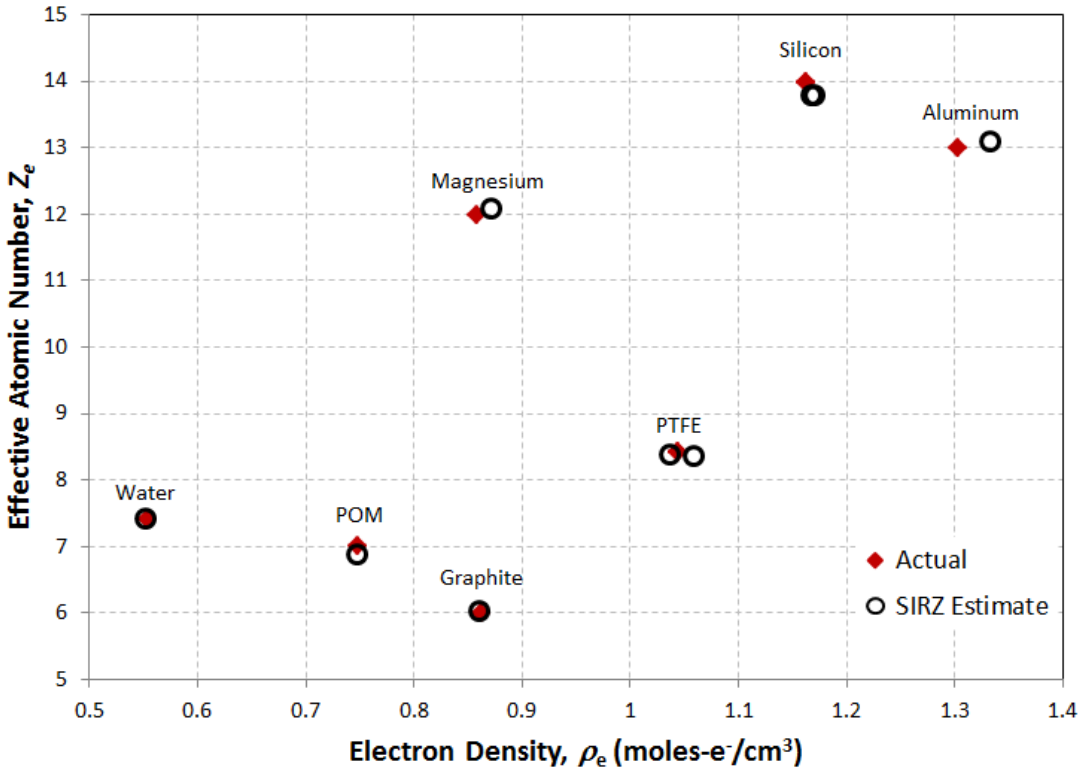

Figure 2. SIRZ results for the specimens tabulated in Table 2.

3.3 SIRZ Applied to Security Applications

As a results of these and other experiments, the Explosives Division (EXD) of the Department of Homeland Security (DHS) and Transportation Security Agency (TSA) have agreed to use (ρ_e, Z_e) features, among other X-ray and physical features, to define signatures of explosives and other threats in order to detect them from non-threats. These features may play a key role in the performance evaluation of Explosive Detection Systems (EDS's) with respect to probabilities of detection (P_D) and false alarm (P_{FA}), and for throughput. A part of our effort to make SIRZ generally usable, particularly for security applications of interest to DHS, is to establish a procedure for ensuring measurable and repeatable results for any DECT scanner. Our next step is to demonstrate that SIRZ can be applied to data from a Leidos CT-80DR dual-energy baggage scanner.

4. SUMMARY AND FUTURE WORK

SIRZ is a novel way to process DECT data for obtaining both precise and accurate material properties. Following the early research and development on SIRZ[8] (that showed accuracy <3% and precision <2%), we reported here that the most recent results on a different scanner were similar (accuracy less than 2%), which meets our current program requirements. SIRZ has been automated into the software package LTT and it was validated against many prior results. We introduced here the LTT implementation, along with a common set of pre-processing algorithms that enhance its accuracy, precision, robustness, portability and speed.

This paper has shown that for applications in security and nondestructive characterization (NDC) where correct knowledge of physical properties would provide improved detection (of explosives or anomalies), the SIRZ method is an ideal choice. It has been demonstrated to be well-suited for important material ranges where $6 \leq Z_e \leq 14$ and $0.5 \leq \rho_e \leq 1.2$, although we anticipate that more expansive ranges are possible with other spectral pairings and reference materials.

We continue to develop the SIRZ technique and algorithm for eventual roll-out to other NDC and security DECT applications. Future work includes extending SIRZ to a broader range of specimens and DECT scanners, including commercial systems such as the Leidos CT-80DR for checked-baggage scanning in airports. We also plan to explore the limitations of SIRZ in cases of specimens outside of the ρ_e and Z_e range of the reference materials (e.g., high-Z materials), or where spectral models are unknown or changing. Finally, we plan to transition the use of SIRZ to diverse characterization applications in the NDC and security domains.

ACKNOWLEDGMENTS

The authors would like to acknowledge the efforts of W. D. Brown, S. DePiero, A. Dooraghi, D. Grimsley, J. S. Kallman, K. Morales, and J. Montgomery in preparing the specimens, acquiring X-ray data, performing analysis and carefully archiving the results to be analyzed and described in this paper. They would like to thank PerkinElmer, Inc., for providing details about their detector array panels.

REFERENCES

[1] Engler, P., Friedman, W. D. and Armstrong, E. E., "Determination of material composition using dual energy computed tomography on a medical scanner," in Proc. ASNT Topical Conf. Industrial Computerized Tomography, 142 (July 1989).

[2] Ying, Z., Naidu, R., and Crawford, C. R., "Dual energy computed tomography for explosive detection," J. X-ray Sci. and Tech., 14, 235–256 (2006).

[3] Robert-Coutant, C., Moulin, V., Sauze, R., Rizo, P. and Casagrande, J.-M., "Estimation of the matrix attenuation in heterogeneous radioactive waste drums using dual-energy computed tomography," Nucl. Inst. Meth., A422, 949–956 (February 1999).

[4] Martz, H. E. Jr., Azevedo, S. G., Brase, J. M., Waltjen, K. E. and Schneberk, D. J., "Computed tomography systems and their industrial applications," Appl. Radiat. Isot., 41, 943 (1990).

[5] Alvarez, R. E. and Macovski, A., "Energy selective reconstructions in x-ray computerized tomography," Phys. Med. Biol., 21 (5), 733–744 (1976).
[6] Lehmann, L. A., Alvarez, R. E., Macovski, A., Brody, W. R., Pelc, N. J., Riederer, S. J. and Hall, A. L., "Generalized image combinations in dual KVP digital radiography," Med. Phys., 8(5), 659–667 (1981).
[7] Kalender, W. A., Perman, W. H., Vetter, J. R. and Klotz, E., "Evaluation of a prototype dual-energy computed tomographic apparatus. I. phantom studies," Med. Phys., 13(3), 334–339 (May/Jun 1986).
[8] Azevedo, S. G., Martz, H. E., Aufderheide, M. B., Brown, W. D., Champley, K. M., Kallman, J. S., Roberson, G. P., Schneberk, D., Seetho, I. M. and Smith, J. A., "System-independent characterization of materials using dual-energy computed tomography," IEEE Trans. Nuc. Sci., 63(1), 341-350 (2016).
[9] Mayneord, M. V., "The significance of the roentgen," Acta of the International Union Against Cancer, ii, 271 (1937).
[10] Champley, K. M., "Livermore Tomography Tools (LTT) Technical Manual", LLNL Technical Report under development, (Dec 11, 2015).
[11] Cullen, D. E., Hubbell, J. H. and Kissel, L., EPDL97: The evaluated photon data library '97 version, LLNL Tech. Rep., UCRL-ID-50400, vol. 6, rev. 5 (Sep. 1997).
[12] Landry, G., Seco, J., Gaudreault, M., and Verhaegen, F., "Deriving effective atomic numbers from DECT based on a parameterization of the ratio of high and low linear attenuation coefficients," Phys. Med. Biol., 58, 6851–6866 (2013).
[13] Bond, K. C., Smith, J. A., Treuer, J. N., Azevedo, S., Kallman, J. S. and Martz, H. E., ZeCalc Algorithm Details, Version 6, LLNL Tech. Rep., LLNL-TR-609327, (Jan. 2013). To request a copy of ZeCalc software, contact Mary Holden-Sanchez at holdensanchez2@llnl.gov.
[14] Poludniowski, G. G. and Evans, P. M., "Calculation of x-ray spectra emerging from an x-ray tube. Part I. electron penetration characteristics in x-ray targets," Med. Phys., 34 (6), 2164–2174 (2007).
[15] Finkelshtein, A. L. and Pavlova, T. O., "Calculation of x-ray tube spectral distributions," X-Ray Spectrom., 28 (1), 27–32 (1999).
[16] Goorley, T., James, M., Booth, T., Brown, F., Bull, J., Cox, L. J., Durkee, J., Elson, J., Fensin, M., Forster, R. A., Hendricks, J., Hughes, H. G., Johns, R., Kiedrowski, B., Martz, R., Mashnik, S., McKinney, G., Pelowitz, D., Prael, R., Sweezy, J., Waters, L., Wilcox, T. and Zukaitis, T., "Features of MCNP6," presented at the J. Int. Conf. Supercomputing in Nuclear Applications and Monte Carlo, Paris, France (Oct. 2013).
[17] Nishioka, A., Matsumae, K., Watanabe, M., Tajima, M., and Owaki, M., "Effects of gamma radiation on some physical properties of polytetrafluoroethylene resin," Journal of Applied Polymer Science, II (4), 114-119 (1959).
[18] Yu, Z., Thibault, J-B., Sauer, K., Bouman, C., and Hsieh, J., "Accelerated line search for coordinate descent optimization," IEEE Nuc. Sci. Symp. Conference Record, pp. 2841-2844 (2006).
[19] Chen, G-H., Tang, J., and Leng, S., "Prior image constrained compressed sensing (PICCS): A method to accurately reconstruct dynamic CT images from highly undersampled projection data sets," Med. Phys., 35:660-663 (2008).
[20] Champley, K. M., and Martz, H. E., "Statistical-analytic regularized reconstruction for x-ray CT," 12th Int'l Meeting on Fully Three-Dimensional Image Reconstruction in Radiology and Nuclear Medicine, pp. 173-176 (2012).
[21] ImageJ open-access Java image processing and analysis software is available from the National Institutes of Health (NIH) at http://imagej.nih.gov/ij/ (accessed March 8, 2016).